Wang *et al.*
*European Journal of Medical Research* (2025) 30:227
https://doi.org/10.1186/s40001-025-02491-w

European Journal of Medical Research

RESEARCH

Open Access

# Inducing mononuclear cells of patients with CADASIL to construct a CSVD disease model

Zhiqiang Wang[1,2,3], Jianjian Yin[4], Wa Chao[2,3] and Xiaoning Zhang[1*]

## Abstract

**Objective** To produce pluripotent stem cells from peripheral blood mononuclear cells (PBMCs) of a patient with cerebral autosomal dominant arteriopathy with subcortical infarcts and leukoencephalopathy (CADASIL) and culture and differentiate them into vascular organoids, producing a disease model for cerebral small vessel disease (CSVD).

**Methods** (1) PMBCs from patients clinically diagnosed with CADASIL (*NOTCH3* p.R141C) were induced to differentiate into pluripotent stem cells (iPSCs); the quality and differentiation ability of the iPSCs were determined. (2) CADASIL-derived iPSCs and control iPSCs were cultured and differentiated into vascular organoids. The differences in the morphological structure of the two differentiated groups of vascular organoids were observed, and both were identified.

**Results** (1) No mycoplasma infections were detected in the iPSCs prepared from the PBMCs of patients with CADASIL. The short tandem repeat (STR) identification verified that the iPSCs originated from the patient, and the karyotype was normal. Flow cytometry and immunofluorescence detection revealed that the iPSCs expressed SSEA4, OCT4, and NANOG stem proteins. Tri-germ differentiation testing confirmed that the iPSCs expressed the endoderm markers SOX17 and FOXA2, the mesoderm markers Brachyury and α-SMA, and the ectoderm markers Pax6 and β-III Tubulin. (2) CADASIL-derived iPSCs and control iPSCs were induced to differentiate and produce endothelial networks and vascular networks, ultimately forming vascular organoids. Compared with control vascular organoids, CADASIL vascular organoids exhibited lower growth density, earlier blood vessel sprouting, longer and thinner vascular filaments, and smaller final vascular organoids. The vascular organoids from the two sources expressed the endothelial cell marker CD31, the vascular smooth muscle marker α-SMA, and the pericyte marker PDGFR-β.

**Conclusion** Reprogramming technology can be used to induce PBMCs to become iPSCs, and a CSVD disease model can be successfully constructed by culturing and differentiating the iPSCs into CADASIL vascular organoids. The *NOTCH3* p.R141C mutation suppresses the vascular differentiation process in CADASIL.

**Keywords** Vascular organoids, Induced pluripotent stem cells, CADASIL, Cerebral small vessel disease

*Correspondence:
Xiaoning Zhang
zhangxn1960@126.com
Full list of author information is available at the end of the article

## Introduction

Cerebral small vessel disease (CSVD) manifests clinically through progressive cognitive decline and gait disturbances, with characteristic neuroimaging findings reflecting pathological alterations in cerebral microvasculature including small arteries, arterioles, venules, and capillaries [1, 2]. As a predominant contributor to vascular cognitive impairment and senile dementia [3], CSVD's insidious progression often leads to delayed diagnosis and underestimation of disease burden [4]. The elucidation of CSVD pathogenesis remains an urgent priority in neurology research due to current limitations in mechanistic understanding and therapeutic interventions [5].

Cerebral Autosomal Dominant Arteriopathy with Subcortical Infarcts and Leukoencephalopathy (CADASIL), a monogenic CSVD subtype caused by NOTCH3 mutations [6], typically manifests in early adulthood (25–35 years). The NOTCH3 gene encodes a transmembrane receptor critical for vascular smooth muscle cell (VSMC) and pericyte homeostasis [7, 8]. Pathogenic mutations induce protein misfolding, leading to three hallmark pathological features: NOTCH3 extracellular domain (N3ECD) accumulation, granular osmiophilic material (GOM) deposition, and progressive VSMC degeneration—collectively demonstrating NOTCH3 mutation-associated vasculopathy [9–11].

Current CADASIL research faces two critical challenges: (1) Existing animal models (stroke-prone SHR rats [12], vasoconstrictor injection models [13]) predominantly reflect large vessel pathology rather than authentic CSVD mechanisms; (2) Traditional 2D in vitro systems fail to recapitulate 3D neurovascular architecture [14]. To address these translational limitations, induced pluripotent stem cell (iPSC) technology has emerged as a promising platform for developing CADASIL-specific in vitro models [15, 16]. Recent breakthroughs demonstrate that CADASIL patient-derived iPSCs generate VSMCs with characteristic disease phenotypes: aberrant proliferation, cytoskeletal disorganization, and dysregulated NOTCH/NF-κB signaling [17]. Genetic correction of NOTCH3 mutations reverses these pathological changes, validating the disease-modeling capacity of iPSC-derived vascular cells [18].

The advent of 3D vascular organoid technology represents a paradigm shift in CSVD modeling. Wimmer et al. pioneered an iPSC-derived vascular organoid system that recapitulates human vasculogenesis, angiogenesis, and vascular maturation processes [19]. This cost-effective platform [20] enables human-specific investigation of vascular pathophysiology without animal experimentation. Notably, NOTCH3-mutant vascular organoids developed by Ahn et al. [21] successfully mimicked key CADASIL features: microvascular stenosis, VSMC degeneration, and N3ECD/GOM deposition. Pharmacological inhibition of ROCK signaling partially rescued endothelial-pericyte interactions in these mutant organoids, suggesting therapeutic potential [21]. Complementary work by Wang et al. [18] identified downregulated pathways in CADASIL organoids involving cell adhesion, extracellular matrix organization, and vascular development.

Building upon these advancements, our study establishes a novel 3D vascular organoid model using iPSCs derived from CADASIL patients carrying the NOTCH3 p.R141C mutation [22, 23]. By incorporating patient-derived peripheral blood mononuclear cells (PBMCs), this bioengineered system simulates the complex neurovascular microenvironment of CSVD in vitro. This innovative model provides a physiologically relevant platform for mechanistic investigations and therapeutic screening in hereditary CSVD.

## Objects and methods

### Participant inclusion

The patient selected for this study was a man with good health and no history of hypertension or diabetes. His father died of cerebral infarction, his mother was in good health, and his sister had a history of migraine. After a physical examination revealed liver hydatid disease, the patient underwent liver hydatid surgery under general anesthesia. Subsequently, he developed lethargy, coughing when drinking water, and dysarthria; his limb muscle strength was grade IV. Brain magnetic resonance imaging (MRI) showed acute lacunar infarction and white matter lesions. Second-generation sequencing of peripheral venous blood revealed a NOTCH3 mutation on Chr19 (15,303,029, c.421C > T, p.R141C). In line with the 2021 Chinese expert consensus on CSVD [24], the patient was diagnosed with CADASIL.

The healthy male control iPSCs were purchased from Guidon Pharmaceutics Ltd (Beijing,China HeFei, China).

The peripheral blood samples involved in this study were collected after fully informing the patient and his family and obtaining their consent. The patient and his family understood the purpose, experimental process, and possible risks of the study and they were ensured that the samples would only be used for scientific research purposes. To protect the patient's privacy and personal information, all sample information was kept strictly confidential. The patient voluntarily signed an informed consent form, and the study was approved by the Ethics Committee of the Second Affiliated Hospital of Xinjiang Medical University (approval number: KY2023112103).

### Reprogramming of PBMCs

Peripheral venous blood was collected from the CADASIL patient by BD Vacutainer® CPT™ Mononuclear Cell Preparation Tube(BD,USA). PBMCs were isolated by Ficoll-Paque Reagent, cultured in chemically defined expansion medium (Help Stem Cell Innovation, China), and then reprogrammed with CytoTune 2.0 Sendai Reprog-ramming Kit (Thermo Fisher Scientific, USA), according to the manufacturer's standardized protocol. Following a four-day expansion period in culture medium, transfected PBMCs were transitioned to differentiation conditions on day 4 by transferring cells to Geltrex-coated wells (Thermo Fisher, USA) in 2 mL StemPro-34 complete medium (Thermo Fisher, USA). Medium replacement with Essential 8 formulation (Thermo Fisher, USA) occurred at day 7 of culture. Between days 17–20, emerging hiPSC colonies displaying characteristic morphology were manually isolated and re-seeded onto fresh Geltrex substrate for clonal expansion. Selected colonies (5–6 lines demonstrating optimal growth characteristics) underwent routine maintenance using Essential 8 medium with bi-weekly passaging (4–7 day intervals) through Gentle Cell Dissociation Reagent (Stem Cell Technologies, Canada) at a 1:3 split ratio. Continuous monitoring ensured proper colony morphology maintenance throughout the reprogramming and expansion phases.

### Immunocytochemistry of hiPSCs

Following a 4-day culture period in Essential 8 medium, CADASIL hiPSC lines underwent sequential immunostaining procedures. Cells were first fixed with 4% paraformaldehyde (PFA) for 5 min at room temperature (RT). Subsequent permeabilization was performed using phosphate-buffered saline (PBS) supplemented with 0.1% saponin and 1% normal donkey serum (NDS) for 15 min at RT. Blocking was achieved by incubating cells in PBS containing 0.05% saponin and 5% NDS for an additional 15 min at RT. Primary antibodies were applied to the samples and incubated overnight at 4 °C, followed by 1-h exposure to fluorophore-conjugated secondary antibodies under RT conditions. All steps adhered to standardized protocols for intracellular antigen detection in pluripotent stem cells. Anti-OCT3/4 antibody,anti-PDGFR-β antibody and anti-α-SMA antibody were purchased from abcam(England).

### Flow cytometry analysis

CADASIL hiPSC cultures were enzymatically dissociated using Accutase (Chemicon, USA) and subjected to three PBS washes. Cell suspensions were adjusted to a final density of 3–5×10^6 cells/mL in PBS supplemented with 1% bovine serum albumin (BSA). For surface marker analysis, fluorochrome-conjugated monoclonal antibodies (PE anti-OCT3/4, PE anti-Nanog, and PE anti-SSEA4,BD,USA) were incubated with cell aliquots under light-protected conditions on ice for 15 min. Following two additional PBS washes, labeled cells were resuspended at $1–2\times10^6$ cells/mL and analyzed using a CytoFLEX flow cytometer (Beckman Coulter, Brea, CA, USA) with instrument parameters standardized via CytoExpert software (v2.4).

### Karyotyping analysis

CADASIL hiPSC cultures were synchronized using colchicine (0.1 μg/mL, 2–4 h), followed by enzymatic dissociation with Accutase (Chemicon, USA). Cells underwent hypotonic treatment with 75 mM KCl for 20 min at 37 °C and subsequent fixation in freshly prepared Carnoy's fixative (methanol:acetic acid, 3:1 v/v). Air-dried metaphase spreads were stained with 4% Giemsa solution (Sigma-Aldrich) for 15 min at room temperature. Chromosomal integrity was assessed by G-banding analysis of 20 high-resolution metaphase spreads using a fully automated karyotyping system (Olympus, Japan).

### Genetic authentication via STR profiling

To confirm genetic identity between CADASIL hiPSC lines and their parental PBMCs, short tandem repeat (STR) analysis was conducted by scilinkbio (Jiangsu, China). Genomic DNA was extracted from passage 10 hiPSCs and donor-matched PBMCs using the DNeasy Blood & Tissue Kit (Vazyme, Nanjing, China). Amplification of 21 autosomal STR loci was performed with the PowerPlex 21 System (Promega, USA), followed by fragment separation on an ABI 3100 Genetic Analyzer (Applied Biosystems,USA). Allelic profiles were cross-compared using GeneMapper ID v3.2.1 software to verify lineage integrity and rule out cross-contamination.

### Mycoplasma screening

All PBMC-derived CADASIL hiPSC lines underwent routine microbiological screening using the Mycoplasma PCR Detection Kit (ExCellBio, Shanghai, China,). Genomic extracts were subjected to Mycoplasma-specific 16S rRNA gene amplification (primers provided in the commercial kit), followed by electrophoretic resolution of PCR products on 1.5% agarose gels. Assay validation included positive controls (Mycoplasma genomic DNA) and no-template negative controls. Absence of mycoplasma contamination was confirmed by the lack of 270–300 bp amplification bands under UV visualization. All procedures strictly followed the manufacturer's standardized thermal cycling parameters and electrophoresis conditions.

### Trilineage differentiation capacity assessment

The pluripotent differentiation potential of CADASIL hiPSC lines was evaluated using the STEMdiff™ Trilineage Differentiation Kit (Stemcell Technologies, Canada) according to the manufacturer's standardized protocol. Differentiated cells representing ectodermal, mesodermal, and endodermal lineages were fixed in 4% paraformaldehyde (PFA) for 15 min at room temperature. Immunocytochemical analysis was performed using lineage-specific primary antibodies: anti-SOX17 and FOXA2 (1:200, ectoderm; Abcam, England), anti-Brachyury and α-SMA (1:200, mesoderm; abcam), Pax6 and β-III Tubulin (1:200, endoderm; abcam). Following overnight incubation at 4 °C, Alexa Fluor-conjugated secondary antibodies (Thermo Fisher, 1:1000) were applied for 1 h at RT. Nuclei were counterstained with DAPI (1 μg/mL) for 5 min. Fluorescence images were acquired using a confocal microscope (Leica TCS SP8) and analyzed with LAS X software (v3.5.7).

### Generation of blood vessel organoids

CADASIL and control iPSCs were enzymatically dissociated into single-cell suspensions using Accutase (Stemcell Technologies, Canada) and seeded at a density of 1,000 cells/well in AggreWell™ EB Formation Medium (Stemcell Technologies) supplemented with 50 μM Rock inhibitor (Y-27632). Embryoid bodies (EBs) formed over 48–72 h were subsequently induced with N2B27 differentiation medium containing 12 μM CHIR99021 (GSK3β inhibitor) and 30 ng/mL BMP4 for 72 h.

On day 5 of differentiation, cultures were transitioned to N2B27 basal medium supplemented with 2 μM Forskolin (Biogem, USA) and 100 ng/mL VEGF165 (Peprotech, USA). Vascular networks (20–30 structures per 2 $cm^2$) were manually isolated, embedded in growth factor-reduced Matrigel (Corning, USA), and cultured in vascular sprouting medium (VSM): StemPro-34 (Gibco, USA) supplemented with 15% fetal bovine serum (FBS), 100 ng/mL VEGF165, and 100 ng/mL FGF2 (RnD Systems, USA).

For organoid maturation, endothelial sprouting regions were mechanically dissociated using sterile 27-gauge needles and transferred to 96-well ultra-low attachment plates (Corning,USA) containing fresh VSM. Blood vessel organoids were maintained under hypoxic conditions (5% $O_2$, 37 °C) with medium replenishment every 48 h.

### Multiplex immunohistochemistry

Blood vessel organoids were fixed by 4% PFA.,then they underwent sequential multiplex staining using an optimized panel of primary antibodies (CD31, PDGFR-β and α-SMA abcam, England) combined with the Opal™ Fluorescent IHC Kit (PerkinElmer,USA). Following deparaffinization in xylene and graded ethanol series (100%–25%), antigen retrieval was performed via microwave heating in citrate buffer (pH 6.0, 95 °C, 20 min). Endogenous peroxidase activity was quenched with 3% H2O2 (10 min, RT), and nonspecific binding was minimized by blocking with 5% normal goat serum (1 h, RT). Primary antibodies were applied sequentially in pre-titrated concentrations, each followed by HRP-conjugated secondary antibodies (30 min, RT) and Opal fluorophores (1:100 dilution;10 min, RT), with intermediate microwave-mediated antibody stripping (95 °C, 10 min) to eliminate cross-reactivity. Nuclei were counterstained with DAPI (Servicebio, Wuhan, China). Multispectral imaging was performed on a Vectra® Polaris system (PerkinElmer), and spectral unmixing was conducted with inForm® software (v2.8) using reference libraries generated from single-stained controls.

### TUNEL assay

Apoptotic activity in blood vessel organoids was evaluated through terminal deoxynucleotidyl transferase dUTP nick-end labeling (TUNEL) methodology. Utilizing the commercial TUNEL detection system (servicebio, Wuhan,China), specimens underwent fixation in 4% paraformaldehyde for 30 min followed by triple PBS rinses. Blood vessel organoids tissue permeabilization was achieved through 20-min Proteinase K (20 μg/mL) digestion at 37 °C. Slides were subsequently equilibrated with reaction buffer for 30 min at ambient temperature prior to enzymatic labeling. The labeling protocol involved sequential application of TdT-mediated dUTP-biotin nick end labeling mixture and nuclear counterstaining with 1 μg/mL DAPI (Servicebio, Wuhan, China). For blood vessel organoids sections exclusively, an additional incubation step with TRITC-conjugated streptavidin (1:200 dilution) was performed under light-protected conditions at 37 °C for 30 min prior to nuclear staining. Fluorescence visualization was conducted using an epifluorescence microscope equipped with appropriate filter sets, with all post-staining procedures executed under minimal light exposure to preserve fluorophore integrity.

### Enzyme-linked immunosorbent assay(ELISA)

Quantification of inflammatory mediators was performed using ELISA to analyze cytokine levels in blood vessel organoids. Commercial ELISA kits from servicebio (Wuhan, China) were employed for specific detection of interleukin (IL)−1β, tumor necrosis factor (TNF)-α, IL-6, IL-18, and IL-10. Prior to assay initiation, all reagents were equilibrated at room temperature for 30 min and reconstituted following the manufacturer's protocols. Samples and standards were loaded into antibody-precoated microplates alongside assay-specific buffers,

followed by sequential incubation steps for antigen–antibody binding, enzymatic conjugation, and substrate conversion. Chromogenic development was initiated by tetramethylbenzidine (TMB) incubation at 37 °C for 15–30 min, with reactions terminated using 2 M sulfuric acid. Absorbance measurements at 450 nm (reference wavelength 570 nm) were acquired using a Bio-Tek MB-530 microplate reader (Heales, Shenzhen, China). Quantitative cytokine concentrations were derived through four-parameter logistic regression analysis of serially diluted calibrators run in parallel. All samples were analyzed in duplicate to ensure technical reproducibility.

#### Transcriptomic profiling

Blood vessel organoids underwent comprehensive RNA sequencing at Novogene Co., Ltd. (Beijing, China). Total RNA isolation was performed using TRIzol reagent, with integrity verification via 1% agarose gel electrophoresis and spectrophotometric analysis (NanoPhotometer®, Implen; OD260/280 ≥ 1.8, OD260/230 ≥ 2.0). RNA integrity numbers (RIN > 8.0) were confirmed using the Agilent 2100 Bioanalyzer (Agilent Technologies). Strand-specific cDNA libraries were prepared from 1 μg rRNA-depleted RNA using the NEBNext Ultra RNA Library Prep Kit (Illumina), incorporating fragmentation, double-stranded cDNA synthesis, end repair, adenylation, and Illumina-compatible adapter ligation. Libraries underwent size selection (350–400 bp) via AMPure XP bead purification (Beckman Coulter), followed by PCR amplification and quantification using RT-qPCR (library concentration > 2 nM).

Sequencing was conducted on the Illumina NovaSeq 6000 platform (PE150 mode) with a minimum output of 6 Gb per sample. Raw data preprocessing involved adapter trimming and quality filtering using Perl 6 scripts to eliminate reads containing ambiguous bases (> 0.2%) or low-quality sequences (*Q*-score < 20 in > 50% of bases). High-confidence clean reads were retained based on stringent quality metrics (Q20 > 95%, Q30 > 90%, GC content 48–52%) calculated via Illumina Casava v1.8.

Bioinformatic analysis employed the GRCm39 reference genome (NCBI) with hierarchical alignment: HISAT2 v2.0.5 mapped reads to the genome, followed by transcript assembly using StringTie v1.3.3. Differential expression analysis of mRNAs was performed using DESeq2 with FDR-adjusted $p < 0.05$ as significance threshold.

#### Statistical analysis

Statistical analyses were conducted using GraphPad Prism 9.0 (GraphPad Software, USA). Continuous data are expressed as mean ± standard deviation (SD). Normality and homogeneity of variance were confirmed prior to parametric testing. Inter-group comparisons were performed using two-tailed Student's *t*-tests for pairwise analyses, while one-way analysis of variance (ANOVA) with Tukey's post hoc correction was applied for multi-group comparisons. Statistical significance was defined as $p < 0.05$ for all analyses.

## Results

#### Generation and characterization of iPSCs

The reprogramming of PBMCs from a patient with CADASIL allowed multiple iPSCs lines to be cultured; four lines with relatively good growth status were obtained and named W1-1, W1-3, W1-7, and W1-8 (Fig. 1A). Under the microscope, we observed that aggregated clumps derived from mononuclear cells and pluripotent stem cells grew in a tightly connected, three-dimensional growth pattern without differentiated cells. The borders of the clonal colonies were clear and smooth.

The STR test results revealed that the PBMC STR loci before reprogramming and the iPSC STR loci after reprogramming (Table 1) were the same, indicating that the two sources were consistent.

The mycoplasma test results revealed no amplification in the negative control and two bands in the positive control. The amplified bands of the iPSC sample were different from those of the positive control, indicating that none of the four lines were infected by mycoplasma (Fig. 1B).

Passage 10 iPSCs were detected G-banding; karyotype analysis was performed after culturing and revealed a normal number of chromosomes (46). The sex chromosomes (XY) reflected a male karyotype, consistent with the patient's gender. Microscopic observation did not reveal any abnormalities in chromosome structure or number (Fig. 1C).

#### Pluripotency assessment and differentiation potential evaluation of stem cells

The stem cell markers SSEA4, OCT4, and NANOG in the iPSC community prepared by flow cytometry all had positive cell rates of over 99% (Fig. 2A); W1-1, W1-3, W1-7, and W1-8 all expressed stemness-related markers.The cell immunofluorescence results revealed positive OCT4 expression in the iPSCs (Fig. 2B).The results of the tri-germ layer differentiation test showed that the cell line expressed the endoderm-specific markers SOX17 and FOXA2, the mesoderm-specific markers Brachyury and α-SMA, and the ectoderm-specific markers Pax6 and β-III Tubulin (Fig. 2C).

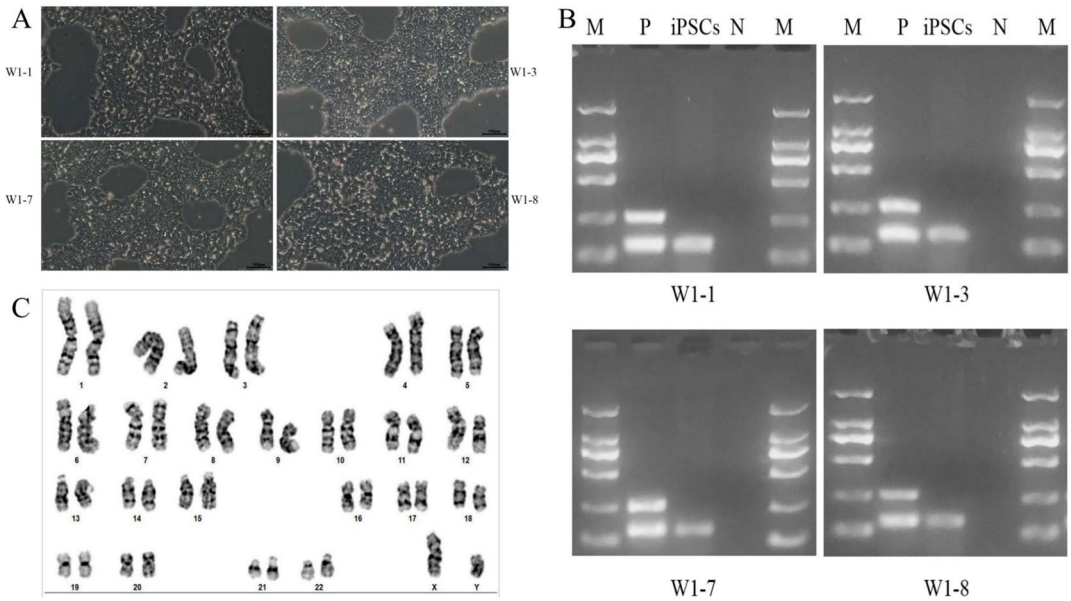


**Fig. 1** Generation and characterization of iPSCs. **A** Different lines lines of iPSCs (200×) named W1-1,W1-3, W1-7 and W1-8. **B** Mycoplasma detection. M: DL2000 marker; P: positive control; iPSCs: induced pluripotent stem cells; N: negative control (ddH2O). C:Chromosome karyotype of P10-generation iPSCs W1-8

**Table 1** Genotyping results of 21-STR locus and amelogenin locus of PBMCs and iPSCs

| STR locus | Allelic genes 1 | Allelic genes 2 | STR locus | Allelic genes 1 | Allelic genes 2 |
|---|---|---|---|---|---|
| D3S1358 | 16 | 16 | TH01 | 7 | 8 |
| vWA | 17 | 19 | D13S317 | 9 | 11 |
| D7S820 | 12 | 13 | TPOX | 8 | 9 |
| CSF1PO | 10 | 12 | D18S51 | 15 | 16 |
| Penta E | 10 | 14 | D6S1043 | 18 | 20 |
| D8S1179 | 14 | 14 | AMEL | X | Y |
| D21S11 | 30 | 32.2 | D1S1656 | 16 | 16 |
| D16S539 | 9 | 9 | D5S818 | 11 | 11 |
| D2S1338 | 19 | 19 | D12S391 | 21 | 21 |
| Penta D | 11 | 12 | FGA | 21 | 22 |
| D19S433 | 14 | 14 | | | |

#### Formation and identification of vascular organoids

The iPSCs were resuscitated and cultured again. After returning to the growth state, the CADASIL and control iPSCs were both observed under a microscope at 4×and 10×. The iPSCs clones were flat with smooth and neat edges, and they were in good condition (Fig. 3A).

We induced iPSCs to differentiate into vascular organoids in vitro and observed this process under a microscope at 4×and 10×. Compared with control vascular organoids, CADASIL vascular organoids had a lower growth density and an earlier blood vessel sprouting time, but the vascular filaments were longer and thinner, and the final vascular organoids were smaller (Fig. 3B).

The immunofluorescence results showed that the vascular organoids expressed the endothelial cell marker CD31 and the pericyte marker PDGFR-β (Fig. 4A). After we verified that the organoids comprised endothelial cells and pericytes, we added the smooth muscle cell marker α-SMA and performed a staining analysis of the three indicators. The results showed that the vascular organoids simultaneously expressed vascular endothelial cells

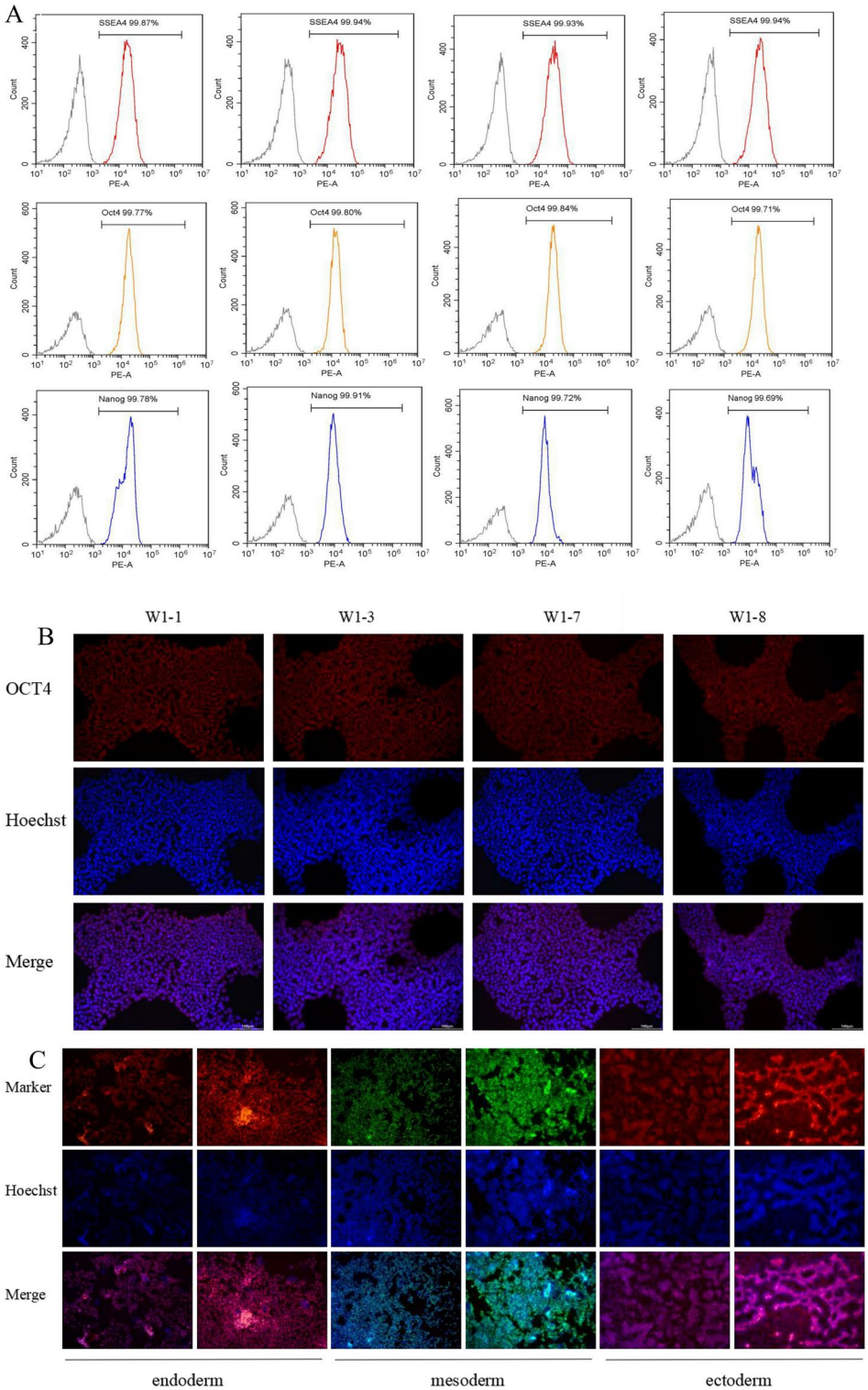


**Fig. 2** iPSC stemness and trilaminar differentiation assays. **A** Flow cytometry: SSEA4 (red), OCT4 (yellow), NANOG (blue).The gray lines represent the results of the isotype control and the colored lines represent the results after adding specific marker detection antibodies; the three stemness markers were significantly expressed in the four iPSC cell lines. **B** Immunofluorescence:OCT4**.**OCT4 is a stemness marker (red), Hoechst is a nuclear stain (blue), and Merge is an overlay of the OCT4 and Hoechst results. **C** Tri-germ layer differentiation test. iPSCs cell lines express endoderm markers SOX17 and FOXA2, mesoderm markers Brachyury and α-SMA, and ectoderm markers Pax6 and β-III Tubulin

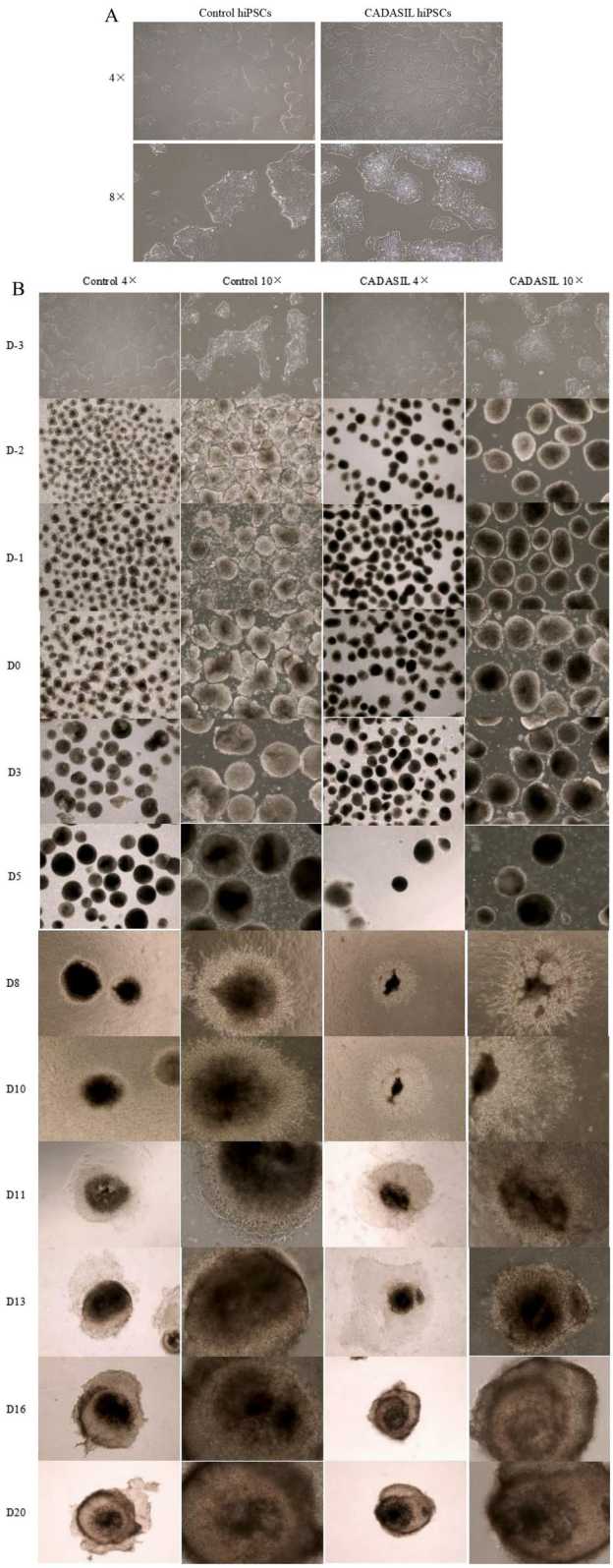


◀ **Fig. 3** Generation of vascular organoids from iPSCs. **A** Status of revived iPSCs in the CADASIL and control groups. **B** D-3 displays the initial morphology of the successfully resuscitated iPSCs in the control group and CADASIL group under 4 × and 10 × magnification; D-2 depicts the digestion of iPSCs into single cells; D-1 and D0 show the aggregation processes of single cells; D3 shows induced vascular mesoderm; D5 shows the beginning of the formation of sprouting blood vessels; D8 shows the beginning of the appearance of an endothelial network; D11 shows the production of a highly branched mature vascular network; and D13–D20 show isolated and continuously cultured single vascular organoids

(CD31), smooth muscle cells (α-SMA), and pericytes (PDGFR-β) in a cell complex structure (Fig. 4B).

### CADASIL NOTCH3 R141C promotes apoptosis by suppressing vascular cell proliferation via oxidative stress

Transmission electron microscopy (TEM) analysis of vascular organoids (Fig. 5A1–A4) revealed severe mitochondrial damage in CADASIL vascular organoids, characterized by reduced mitochondrial numbers and prominent accumulation of autophagic vesicles (indicated by black arrows in Fig. 5A4). To investigate the impact of NOTCH3 R141C on cell proliferation and apoptosis, we performed Ki67 immunofluorescence staining and TUNEL assays. Compared to control vascular organoids, NOTCH3 R141C-mutant organoids exhibited significantly lower Ki67-positive rates and higher numbers of apoptotic cells (Fig. 5A5–A8). Furthermore, total superoxide dismutase (SOD) activity was markedly reduced in CADASIL organoids, while malondialdehyde (MDA) levels were significantly elevated ($P < 0.05$) (Fig. 5B). Notably, IL-1β levels were significantly increased in CADASIL vascular organoids, whereas no significant differences were observed in IL-6, TNF-α, or IL-10 levels between the CADASIL and control groups (Fig. 5B).

### NOTCH3 R141C inhibits microvascular formation through inflammation and oxidative stress

Sequencing analysis revealed 26,228 differentially expressed genes (DEGs) shared between CADASIL vascular organoids and control vascular organoids, comprising 4822 upregulated and 4405 downregulated genes. The distribution of DEGs across comparison groups was visualized using volcano plots (Fig. 6A), with hierarchical clustering patterns displayed in heatmaps (Fig. 6B). Applying thresholds of $|\log2FoldChange| \geq 1$ and $padj < 0.05$ yielded 4946 significant DEGs. The top 30 most enriched Gene Ontology (GO) terms (Fig. 6C)

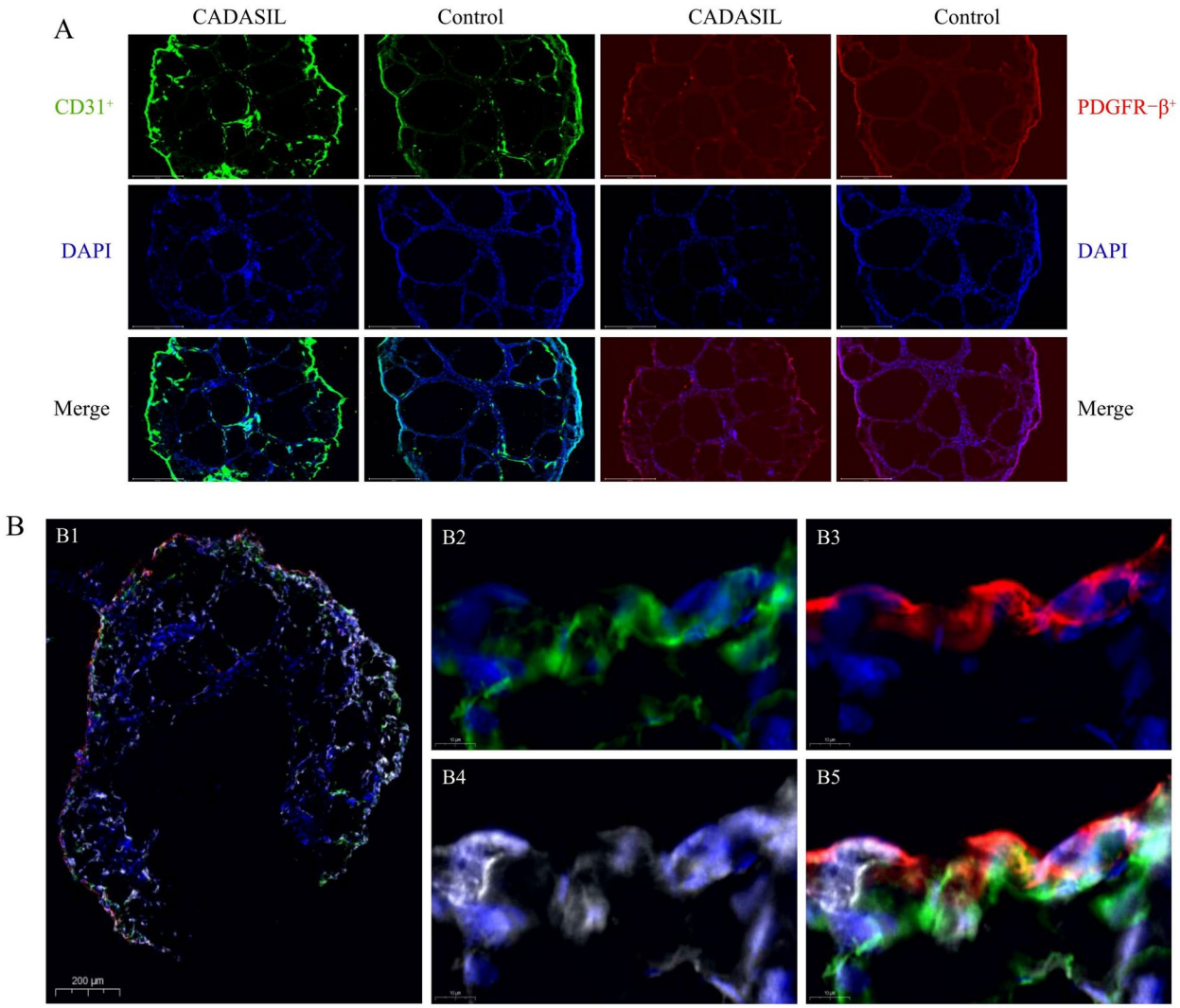


**Fig. 4** Identification of vascular organoids differentiated from iPSCs. Green: α-SMA +; red: CD31 +; white: PDGFR-β +; blue: DAPI. **A** Immunofluorescence:Green (CD31 +), Red (PDGFR-β +) and Blue (DAPI). **B** Multiplex immunofluorescence:Green (α-SMA +), red (CD31 +), white (PDGFR-β +) and blue (DAPI). **B1** The vascular organoid was stained with the vascular smooth muscle cell marker α-SMA, the endothelial cell marker CD31, and the pericyte marker PDGFR-β. **B2** Vascular smooth muscle cell marker α-SMA and DAPI. **B3** Vascular endothelial cell marker CD31 and DAPI. **B4** Vascular pericyte marker PDGFR-β and DAPI.E: Merge of figure B2, B3 and B4

and KEGG pathways (Fig. 6D) were plotted as scatter diagrams.

Significantly enriched biological processes included: regulation of blood vessel diameter (GO:0097746), regulation of blood vessel size (GO:0050880), blood vessel remodeling (GO:0001974), morphogenesis of an epithelium (GO:0002009), morphogenesis of a branching structure (GO:0001763), and epithelial tube morphogenesis (GO:0060562). Cellular component terms featured mitochondrial respiratory chain (GO:0005746), lysosomal lumen (GO:0043202), and mitochondrial protein complex (GO:0005747). Molecular functions demonstrated enrichment in NADH dehydrogenase activity (GO:0003954), protein kinase C binding (GO:0005080), beta-catenin binding (GO:0008013), and ion channel binding (GO:0044325).

KEGG pathway analysis revealed significant enrichment in: TGF-beta signaling pathway (hsa04350), Notch signaling pathway (hsa04330), MAPK signaling pathway (hsa04010), NF-kappa B signaling pathway (hsa04064), Wnt signaling pathway (hsa04310), TNF signaling pathway (hsa04668), and signaling pathways regulating pluripotency of stem cells (hsa04550).

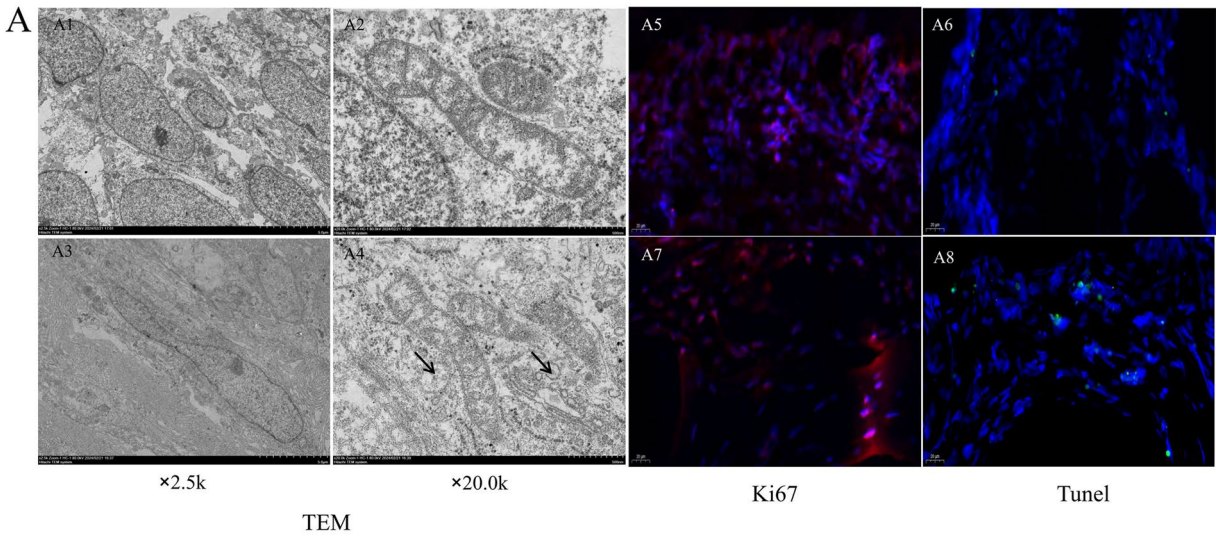


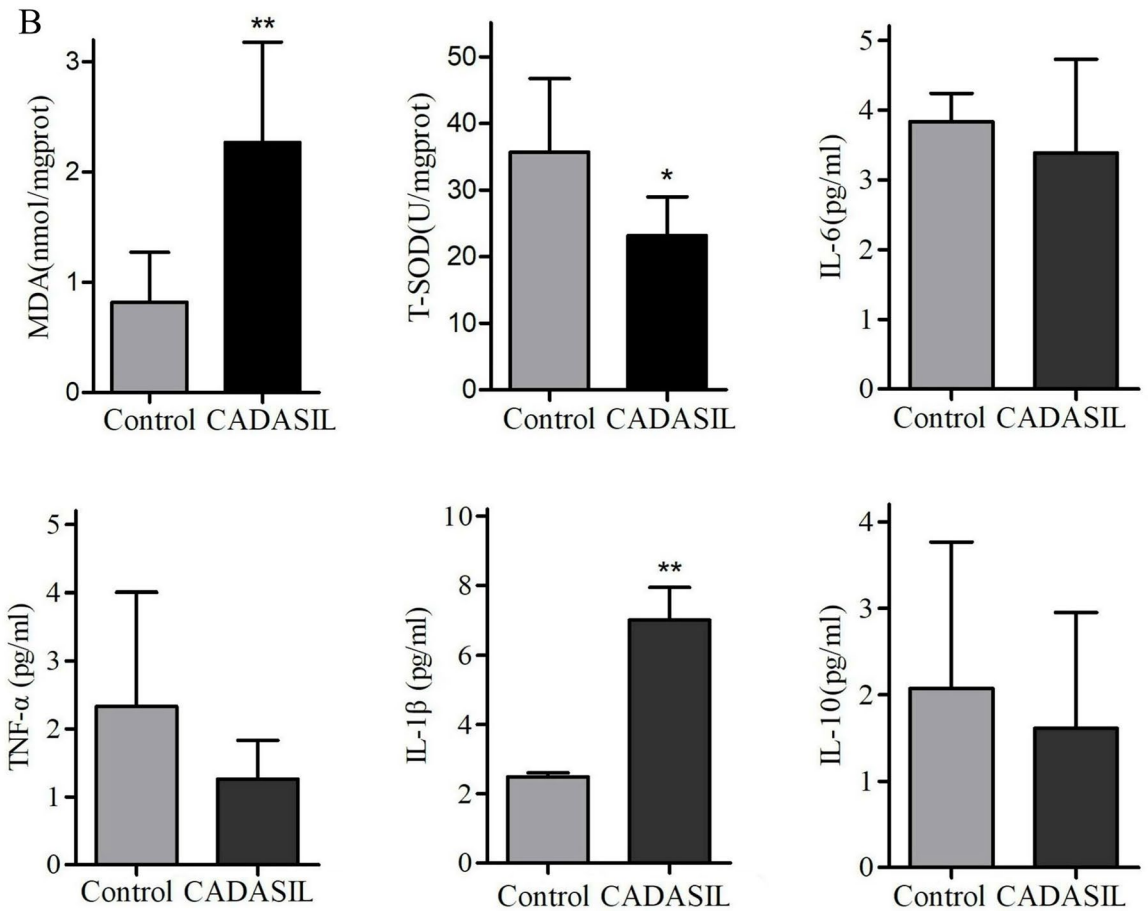


**Fig. 5** NOTCH3 R141C inhibits vascular organoid cell proliferation via oxidative stress and inflammation. **A** NOTCH3 R141C suppresses proliferation and promotes apoptosis. Transmission electron microscopy (TEM) reveals mitochondrial damage: **A1** Control vascular organoids (× 2.5 K); **A2** Control vascular organoids (× 20.0 K); **A3** CADASIL vascular organoids (× 2.5 K); **A4** CADASIL vascular organoids (× 20.0 K), showing severe mitochondrial damage and autophagic vesicles (black arrows). Immunofluorescence staining for Ki67 expression: **A5** Control vascular organoids; **A7** CADASIL vascular organoids, demonstrating reduced Ki67-positive cells. TUNEL assay for apoptotic cells: **A6** CADASIL vascular organoids; **A8** CADASIL vascular organoids, highlighting increased apoptotic signals. **B** NOTCH3 R141C mutation in CADASIL exacerbates oxidative stress and inflammatory response in vascular organoids

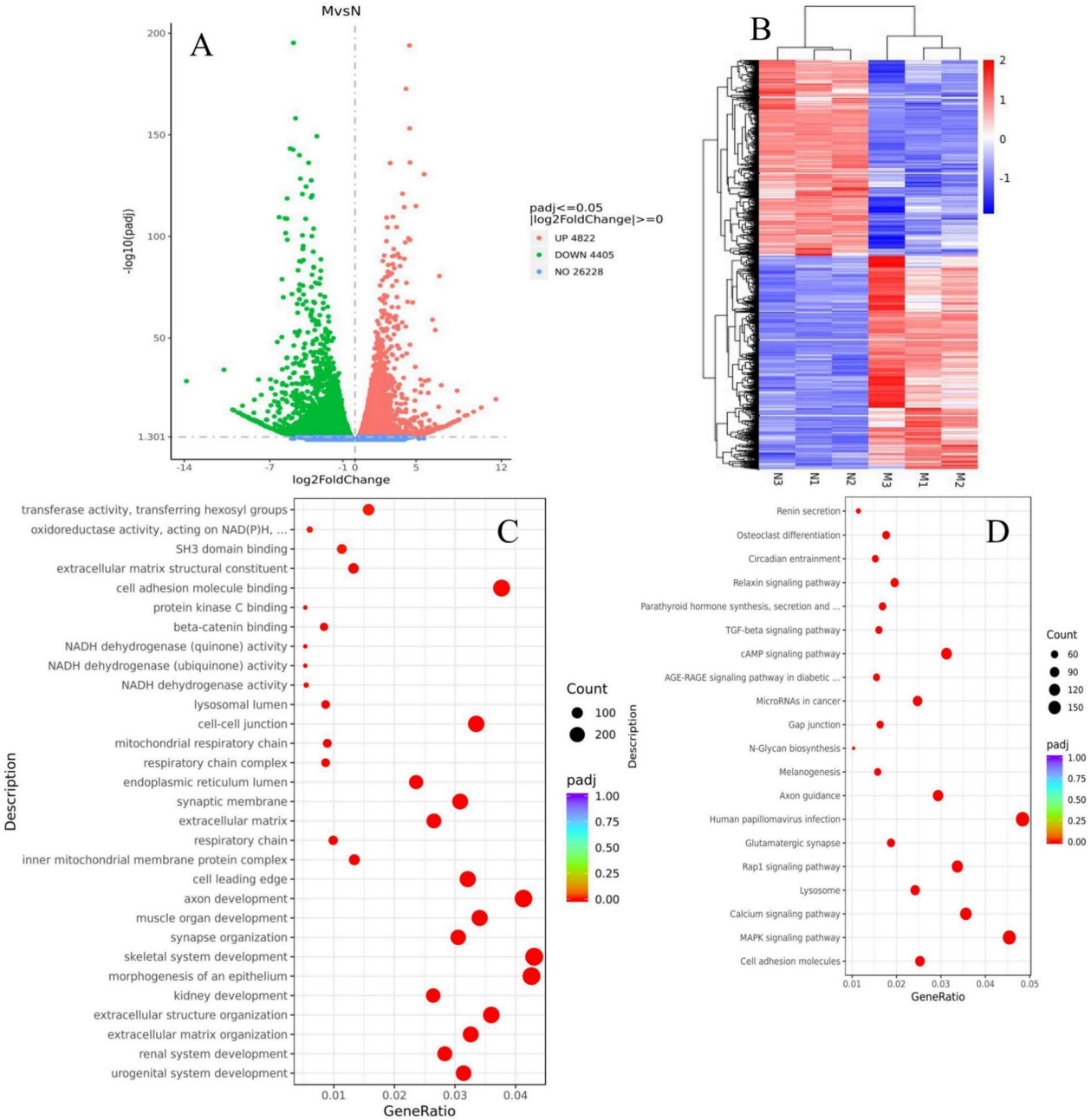


**Fig. 6** Sequencing analysis of CADASIL NOTCH3 R141C vascular organoids and control vascular organoids (M: CADASIL vascular organoids, N: control vascular organoids.) **A** Volcano plot of differentially expressed genes. The abscissa is the fold change of gene expression in the treatment group and the control group (log2 Fold Change), and the ordinate is the significance level of the gene expression difference between the treatment group and the control group (– log10padj). The blue dotted line represents the threshold line of the differential gene screening standard, the red dots represent up-regulated genes, and the green dots represent down-regulated genes. **B** Clustered Heatmap of Differentially Expressed Genes. The abscissa is the sample name, and the ordinate is the normalized value of the differential gene FPKM. The redder the color, the higher the expression level, and the greener the color, the lower the expression level. M1, M2 and M3: CADASIL vascular organoids, N1, N2 and N3: control vascular organoids. **C** Scatter Plot of GO enrichment analysis. **D** Scatter plot of KEGG enrichment analysis

## Discussion

In recent years, organoids have been increasingly used as in vitro disease models because their physiological characteristics are similar to those of humans [25, 26]. Vascular organoids derived from iPSCs can better describe natural physiological and pathological processes

[27, 28] because they contain endothelial cells, parietal cells, smooth muscle cells, and other multicellular populations, and they have become an important tool for studying cardiovascular and cerebrovascular diseases, such as diabetes vascular disease, hypertension, stroke [19, 29].

CADASIL is an inherited CSVD caused by mutations in the NOTCH3 gene [30]. To date, transgenic animal models with NOTCH3 mutations have been studied more than other animal models, and their phenotypes closely mimic the clinical symptoms of patients with CSVD [29]. However, several important clinical phenotypes cannot be reproduced in NOTCH3 transgenic models with different mutation sites [31], so we selected a patient with CADASIL *NOTCH3* p.R141C and used his PBMCs as a starting point. We induced the PBMCs to differentiate into vascular organoids, constructed a CSVD disease model, and performed preliminary work for subsequent research on CSVD pathogenesis.

We used reprogramming technology to successfully induce PBMCs from the CADASIL patient to differentiate into iPSCs and confirmed that the iPSCs were derived from the patient, had a normal karyotype, and were free of mycoplasma infection through STR identification, mycoplasma detection, and karyotype analysis. These findings confirm that our reprogramming method maintained the genetic stability of the cells. The prepared iPSCs expressed stemness-related markers (i.e., SSEA4, OCT4, and NANOG) and had complete endoderm, mesoderm, and ectoderm differentiation capabilities, demonstrating that the prepared iPSCs had good differentiation pluripotency.

The formation of new blood vessels generally involves two processes: vasculogenesis and angiogenesis. Vasculogenesis is the process through which precursor cells in the mesoderm differentiate and assemble into a primitive tubular network known as the capillary plexus, and angiogenesis is the process through which new blood vessels reshape and branch to form a mature vascular network [18]. We successfully obtained vascular organoids by inducing and differentiating iPSCs from a patient with CADASIL *NOTCH3* p.R141C and healthy individuals, and the differentiation process effectively simulated the processes of vasculogenesis and angiogenesis in vivo. Upon examining and comparing the two groups of vascular organoids, we detected some notable differences. The vascular organoids that differentiated from CADASIL iPSCs exhibited lower growth density than those derived from normal iPSCs, indicating that they produced fewer vascular structures from the same number of starting cells. Furthermore, CADASIL vascular organoids exhibited earlier vessel sprouting, which may indicate accelerated differentiation. However, although they sprouted earlier, these vascular organoids were less dense and had longer and thinner vascular filaments, and the final vascular organoids were smaller. These results suggest that the *NOTCH3* p.R141C mutation hinders the vascular differentiation process in CADASIL, resulting in a decrease in both the quantity and quality of the generated vascular structures. The results of the three-label immunofluorescence experiment revealed that all the obtained vascular organoids expressed the endothelial cell marker CD31, the smooth muscle cell marker α-SMA, and the pericyte marker PDGFR-β, and they had a cellular composition similar to that of real blood vessels. These findings indicate that the differentiation into CADASIL vascular organoids and control vascular organoids was successful; therefore, we constructed an accurate CSVD disease model and a control vascular organoid model.

These vascular organoid models can be used to further study vascular biology and disease mechanisms. Such studies would provide a deeper understanding of the complex pathological process of CSVD, lay the foundation for subsequent experiments, and further elucidate CSVD pathogenesis. As technology continues to advance and the application fields expand, vascular organoids are expected to play an increasingly important role. We plan to use this disease model to conduct more innovative studies, promoting the progress of CSVD research and that of other related diseases.

**Acknowledgements**
We also thank Liao Maosen provided technical support for generation of blood vessel organoids.

**Author contributions**
Z W: Conceptualization, Visualization, Writing—original draft, Funding acquisition. J Y: Conceptualization, Writing—original draft, Writing—review and editing. W C: Conceptualization, Visualization, Writing—original draft. X Z: Conceptualization, Writing—review and editing, Supervision.

**Funding**
This work was supported by the Xinjiang Uygur Autonomous Region Natural Science Foundation General Project (2023D01C113). This work was supported by the Xinjiang Medical University, State Key Laboratory of Pathogenesis, Prevention and Treatment of High Incidence Diseases in Central Asia Fund (SKL-HIDCA-2024-GX9).

**Availability of data and materials**
No datasets were generated or analysed during the current study.

## Declarations

**Ethics approval and consent to participate**
The study was approved by the Ethics Committee of the Second Affiliated Hospital of Xinjiang Medical University (approval number: KY2023112103).

**Consent for publication**
The peripheral blood samples involved in this study were collected after fully informing the patient and his family and obtaining their consent. The patient and his family understood the purpose, experimental process, and possible risks of the study and they were ensured that the samples would only be used for scientific research purposes. To protect the patient's privacy and personal information, all sample information was kept strictly confidential. The patient voluntarily signed an informed consent form.

**Competing interests**
The authors declare no competing interests.

**Author details**
[1]The Second Department of Encephalopathy, The Fourth Affiliated Hospital of Xinjiang Medical University, 116 Huanghe Road, Shaybak District, Urumqi 830099, Xinjiang, China. [2]Department of Neurology, Second Affiliated Hospital of Xinjiang Medical University, Urumqi, China. [3]Xinjiang Key Laboratory of Neurological Disorder Research, Urumqi, China. [4]Department of Tumor, First Affiliated Hospital of Xinjiang Medical University, Urumqi, China.

Received: 13 January 2025 Accepted: 21 March 2025
Published online: 02 April 2025

**References**

1. Lu W, Ma Q, Wang J, et al. Association of late-life blood pressure change with cerebral small vessel disease in the MIND-China study. Eur J Med Res. 2024;29(1):372.
2. Mooldijk SS, Ikram MA. Cerebral small vessel disease in population-based research: what are we looking at-and what not? Aging Dis. 2024;15(4):1438.
3. Wang N, Liang C, Zhang X, et al. Brain structure-function coupling associated with cognitive impairment in cerebral small vessel disease. Front Neurosci. 2023;17:1163274.
4. Hannawi Y. Cerebral small vessel disease: a review of the pathophysiological mechanisms. Transl Stroke Res. 2023. https://doi.org/10.1007/s12975-023-01195-9.
5. Papakonstantinou E, Bacopoulou F, Brouzas D, et al. NOTCH3 and CADASIL syndrome: a genetic and structural overview. EMBnet J. 2019;24:e921.
6. Coupland K, Lendhal U, Karlström H. Role of NOTCH3 mutations in the cerebral small vessel disease cerebral autosomal dominant arteriopathy with subcortical infarcts and leukoencephalopathy. Stroke. 2018;49(11):2793–800.
7. Lin C, Huang Z, Zhou R, et al. Notch3 and its CADASIL mutants differentially regulate cellular phenotypes. Exp Ther Med. 2021;21(2):117.
8. Tarzjani SPC, Fazeli SAS, Sanati MH, et al. Genetic study of the NOTCH3 gene in CADASIL patients. Egypt J Med Hum Genet. 2018;19(4):425–7.
9. Ishiko A, Shimizu A, Nagata E, et al. Notch3 ectodomain is a major component of granular osmiophilic material (GOM) in CADASIL. Acta Neuropathol. 2006;112:333–9.
10. Monet-Leprêtre M, Haddad I, Baron-Menguy C, et al. Abnormal recruitment of extracellular matrix proteins by excess Notch3ECD: a new pathomechanism in CADASIL. Brain. 2013;136(6):1830–45.
11. Manini A, Pantoni L. CADASIL from bench to bedside: disease models and novel therapeutic approaches. Mol Neurobiol. 2021;58(6):2558–73.
12. Morton L, Arndt P, Garza AP, et al. Spatio-temporal dynamics of microglia phenotype in human and murine cSVD: impact of acute and chronic hypertensive states. Acta Neuropathol Commun. 2023;11(1):204.
13. Park IH, Arora N, Huo H, et al. Disease-specific induced pluripotent stem cells. Cell. 2008;134(5):877–86.
14. Ling C, Liu Z, Song M, et al. Modeling CADASIL vascular pathologies with patient-derived induced pluripotent stem cells. Protein Cell. 2019;10(4):249–71.
15. Wang J, Zhang L, Wu G, et al. Correction of a CADASIL point mutation using adenine base editors in hiPSCs and blood vessel organoids. J Genet Genomics. 2024;51(2):197–207.
16. Yamamoto Y, Kojima K, Taura D, et al. Human iPS cell-derived mural cells as an in vitro model of hereditary cerebral small vessel disease. Mol Brain. 2020;13:1–12.
17. Wimmer RA, Leopoldi A, Aichinger M, et al. Generation of blood vessel organoids from human pluripotent stem cells. Nat Protoc. 2019;14(11):3082–100.
18. Salewskij K, Penninger JM. Blood vessel organoids for development and disease. Circ Res. 2023;132(4):498–510.
19. Zhao X, Zhang Z, Zhu Q, et al. Modeling human ectopic pregnancies with trophoblast and vascular organoids. Cell Rep. 2023;42(6): 112546.
20. Ahn Y, An JH, Yang HJ, et al. Blood vessel organoids generated by base editing and harboring single nucleotide variation in Notch3 effectively recapitulate CADASIL-related pathogenesis. Mol Neurobiol. 2024;61(11):9171–83.
21. Abe K, Murakami T, Matsubara E, et al. Clinical features of CADASIL. Ann N Y Acad Sci. 2002;977:266–72.
22. Ni W, Zhang Y, Zhang L, et al. Genetic spectrum of NOTCH3 and clinical phenotype of CADASIL patients in different populations. CNS Neurosci Ther. 2022;28(11):1779–89.
23. Neuroradiology Group of Chinese Society of Radiology of Chinese Medical Association. Expert consensus on the standardized application of MRI in cerebral small vessel diseases . 2024, 58(1): 6–17.
24. Hong ZX, Zhu ST, Li H, et al. Bioengineered skin organoids: from development to applications. Mil Med Res. 2023;10(1):40.
25. An Y, He Y, Ge N, et al. Organoids to remodel SARS-CoV-2 research: updates, limitations and perspectives. Aging Dis. 2023;14(5):1677.
26. Shalek AK, Satija R, Shuga J, et al. Single-cell RNA-seq reveals dynamic paracrine control of cellular variation. Nature. 2014;510(7505):363–9.
27. Ricard N, Bailly S, Guignabert C, et al. The quiescent endothelium: signalling pathways regulating organ-specific endothelial normalcy. Nat Rev Cardiol. 2021;18(8):565–80.
28. Chabriat H, Joutel A, Dichgans M, et al. Cadasil. Lancet Neurol. 2009;8(7):643–53.
29. Oliveira D, Coupland K, Shao W, et al. Active immunotherapy reduces NOTCH3 deposition in brain capillaries in a CADASIL mouse model. EMBO Mol Med. 2023;15(2): e16556.
30. Joutel A. Pathogenesis of CADASIL: transgenic and knock-out mice to probe function and dysfunction of the mutated gene, Notch3, in the cerebrovasculature. BioEssays. 2011;33(1):73–80.
31. Joutel A. Pathogenesis of CADASIL: transgenic and knock-out mice to probe function and dysfunction of the mutated gene, Notch3, in the cerebrovasculature. BioEssays News Rev Mol Cell Dev Biol. 2011;33(1):73–80.

## Publisher's Note